



Elucidating Λ CDM: Impact of Baryon Acoustic Oscillation Measurements on the Hubble Constant Discrepancy

G. E. Addison¹ , D. J. Watts¹ , C. L. Bennett¹ , M. Halpern² , G. Hinshaw² , and J. L. Weiland¹

¹ Dept. of Physics & Astronomy, The John Hopkins University, 3400 N. Charles Street, Baltimore, MD 21218-2686, USA; gaddison@jhu.edu

² Department of Physics and Astronomy, University of British Columbia, 6224 Agricultural Road, Vancouver, BC V6T 1Z1, Canada

Received 2017 July 20; revised 2017 November 16; accepted 2017 December 12; published 2018 January 30

Abstract

We examine the impact of baryon acoustic oscillation (BAO) scale measurements on the discrepancy between the value of the Hubble constant (H_0) inferred from the local distance ladder and that from *Planck* cosmic microwave background (CMB) data. While the BAO data alone cannot constrain H_0 , we show that combining the latest BAO results with *WMAP*, Atacama Cosmology Telescope (ACT), or South Pole Telescope (SPT) CMB data produces values of H_0 that are $2.4\text{--}3.1\sigma$ lower than the distance ladder, independent of *Planck*, and that this downward pull was less apparent in some earlier analyses that used only angle-averaged BAO scale constraints rather than full anisotropic information. At the same time, the combination of BAO and CMB data also disfavors the lower values of H_0 preferred by the *Planck* high-multipole temperature power spectrum. Combining galaxy and $\text{Ly}\alpha$ forest BAO with a precise estimate of the primordial deuterium abundance produces $H_0 = 66.98 \pm 1.18 \text{ km s}^{-1} \text{ Mpc}^{-1}$ for the flat Λ CDM model. This value is completely independent of CMB anisotropy constraints and is 3.0σ lower than the latest distance ladder constraint, although 2.4σ tension also exists between the galaxy BAO and $\text{Ly}\alpha$ BAO. These results show that it is not possible to explain the H_0 disagreement solely with a systematic error specific to the *Planck* data. The fact that tensions remain even after the removal of any single data set makes this intriguing puzzle all the more challenging to resolve.

Key words: cosmic background radiation – cosmological parameters – cosmology: observations – distance scale – large-scale structure of universe

1. Introduction

While no single data set currently provides compelling evidence for a deviation from the standard Lambda cold dark matter (Λ CDM) cosmological model, the values of some parameters inferred from different measurements now exhibit moderate to severe tension. This is most pronounced in the value of the Hubble constant, H_0 . Riess et al. (2016; hereafter R16) provided the most recent and most precise local distance ladder constraint, finding $H_0 = 73.24 \pm 1.74 \text{ km s}^{-1} \text{ Mpc}^{-1}$ by combining three absolute distance anchors with the empirical period–luminosity relation for Cepheid variable stars and the relationship between observed light curve and intrinsic luminosity of type Ia supernovae (SNe). The most precise H_0 prediction from cosmic microwave background (CMB) anisotropy power spectrum measurements is currently provided by the *Planck* mission. The 2015 *Planck* temperature and polarization analysis produced $H_0 = 67.31 \pm 0.96 \text{ km s}^{-1} \text{ Mpc}^{-1}$ (Planck Collaboration et al. 2016a). An updated analysis with a revised estimate of the optical depth to reionization, τ , found $H_0 = 66.88 \pm 0.91$, or 66.93 ± 0.62 if preliminary small-scale polarization data are also included (Planck Collaboration et al. 2016b). Assuming all uncertainties are Gaussian, these values are, respectively, 3.0σ , 3.2σ , and 3.4σ lower than the distance ladder determination. Strong lensing timing delay measurements have produced H_0 constraints consistent with the distance ladder, and in mild tension with *Planck* (Bonvin et al. 2017). Tensions also exist between the *Planck* predictions for the growth of cosmic structure (through the matter density, Ω_m , and present-day density fluctuation amplitude, σ_8) and measurements using weak gravitational lensing (e.g., Alsing et al. 2017; Hildebrandt et al. 2017; Joudaki et al. 2017; Köhlinger et al. 2017).

It is not clear whether the problem is with the model or the data. While it is certainly plausible that a failure of the standard model could show up as a discrepancy between the CMB and low-redshift measurements, none of the commonly considered or physically motivated extensions to Λ CDM appear to provide a convincing improvement when considering the full range of data available (e.g., Bernal et al. 2016; Planck Collaboration et al. 2016a). In principle, the CMB prediction for H_0 could be significantly increased by modifying the expansion history of the universe post-recombination, for example, by allowing spatial curvature or a dark energy equation of state $w \neq -1$. *Planck* temperature and polarization data alone mildly prefer a non-zero curvature, but H_0 goes in the wrong direction. The *Planck* 2015 Λ CDM + Ω_k constraint is $53.2 \pm 5.1 \text{ km s}^{-1} \text{ Mpc}^{-1}$ (mean and standard deviation), with 95% of Markov chain Monte Carlo (MCMC) samples lying in $43.7 < H_0 / \text{km s}^{-1} \text{ Mpc}^{-1} < 63.5$.³ Allowing $w < -1$ can shift the *Planck* prediction to 70 or even $80 \text{ km s}^{-1} \text{ Mpc}^{-1}$, however, even leaving aside questions of the physical interpretation of $w < -1$, resolving the H_0 disagreement with evolution in w is strongly disfavored when we include observations of the expansion rate, such as baryon acoustic oscillations (BAO) in the clustering of galaxies, or high-redshift SNe. Alam et al. (2017) combined *Planck* data with the latest galaxy clustering and SNe data and found $H_0 = 67.9 \pm 0.9 \text{ km s}^{-1} \text{ Mpc}^{-1}$ for constant w , or $67.5 \pm 1.0 \text{ km s}^{-1} \text{ Mpc}^{-1}$ for the $w_0 - w_a$ parameterization.

Modifying the early-universe expansion history, for instance, by increasing the number of effective neutrino species, N_{eff} , can increase the CMB H_0 prediction. The *Planck* data do not favor this solution, for example, Alam et al. (2017) reported

³ The public *Planck* MCMC chains can be downloaded from the *Planck* legacy archive: <http://pla.esac.esa.int/pla/>.

$N_{\text{eff}} = 2.97 \pm 0.20$ (*Planck*-only), and 3.03 ± 0.18 (*Planck* plus galaxy clustering), consistent with the standard model value of 3.046, with corresponding H_0 constraints of 66.6 ± 1.6 and $67.5 \pm 1.2 \text{ km s}^{-1} \text{ Mpc}^{-1}$. Adding N_{eff} in these fits shifted the tension with the distance ladder from 3.2σ to 2.8σ (*Planck*-only) and from 3.1σ to 2.7σ (*Planck* plus galaxy clustering). A fit to the 2015 *Planck* temperature and polarization data plus BAO fixing $N_{\text{eff}} = 3.4$, the value found by R16 to most effectively relieve *Planck*-distance ladder tension, leads to an increase in the parameter combination best constrained by weak lensing measurements, $\sigma_8 \Omega_m^{0.5}$, by around 1.5%, 0.8 times the original uncertainty.⁴ This slightly worsens the tension between *Planck* and the weak lensing analyses mentioned above, which found $\sigma_8 \Omega_m^{0.5}$ values lower than *Planck* at the 2σ – 3σ level when the standard model was assumed. Brust et al. (2017) found that the *Planck*-lensing consistency could be improved by also introducing some degree of neutrino or dark radiation self-interaction, but even with a second additional parameter, a joint fit to the *Planck*, BAO, distance ladder, weak lensing, and galaxy cluster data produced a H_0 distribution peaking at $69.95 \text{ km s}^{-1} \text{ Mpc}^{-1}$, still almost 2σ lower than the R16 measurement. In short, while a non-standard value of N_{eff} cannot be ruled out, its inclusion is not justified by the improvements to the fit.

On the other hand, the discrepant data sets have passed a range of systematic checks. The R16 distance ladder analysis used infrared data to greatly reduce the effects of reddening, substituted rungs of the ladder with alternative data, compared different calibrators, corrected for estimated local motion, and constructed a systematic error budget from considering a range of modeling variants (see also, e.g., Cardona et al. 2017; Dhawan et al. 2018; Feeney et al. 2017; Follin & Knox 2017; Zhang et al. 2017). The distance ladder measurements have substantially improved since the analysis by Efstathiou (2014). While the constraints have become tighter, the mean H_0 values in recent years have remained fairly constant (e.g., Riess et al. 2009, 2011; Freedman et al. 2012). Likewise, the *Planck* team has performed an array of robustness checks of their data, investigating the effects of detector nonlinearity, beam shapes and sidelobes, and various other calibration-related issues. Also, the preference for a lower H_0 from *Planck* does not appear to be driven by a particular frequency channel (Planck Collaboration et al. 2017).

Ultimately, it may take additional high-precision measurements to shed light on what is really going on. More precise measurements may bring with them new tensions or disagreements, and the handling of systematic errors will get harder, not easier, as statistical uncertainties are reduced. In the meantime, it is therefore helpful to re-examine existing data and ask whether any extra insight into the discrepancies can be gleaned. To this end, in this paper we investigate in detail the indirect but important role played by BAO measurements in H_0 constraints, both with and without CMB anisotropy data. While this topic has been addressed in the literature, we describe several results that have either not previously been discussed, or are not widely appreciated. In Section 2, we review the BAO measurements. In Section 3, we describe results of fitting cosmological parameters to BAO in conjunction with other

data sets, focusing on H_0 . A discussion and conclusions follow in Sections 4 and 5.

2. BAO Measurements

The first convincing detections of the BAO feature in the correlation function or power spectrum of large-scale structure (LSS) tracers were made a little over a decade ago (Cole et al. 2005; Eisenstein et al. 2005). Since that time, deeper surveys with orders of magnitude more galaxies, notably the Baryon Oscillation Spectroscopic Survey (BOSS⁵), have led to both improved precision in the BAO scale measurements over a range of redshifts, and improved analysis methodologies (e.g., Anderson et al. 2014; Kazin et al. 2014; Percival et al. 2014; Reid et al. 2016). While current and future BAO surveys are proposed as a means of improving dark energy constraints, BAO measurements also provide significant information about parameters in the standard Λ CDM model, particularly in joint fits with the CMB.

A detailed discussion of BAO physics can be found in Chapter 4 of Weinberg et al. (2013). The BAO scale in the transverse and line-of-sight direction correspond to measurements of $D_M(z)/r_d$ and $H(z)r_d$, where $D_M(z) = (1+z)D_A(z)$ is the comoving angular diameter distance at the effective redshift of the survey and r_d is the sound horizon at the drag epoch where baryons decouple from photons, denoted z_d . The sound horizon is defined as⁶

$$r_d = \int_{z_d}^{\infty} dz \frac{c_s(z)}{H(z)}, \quad (1)$$

where the sound speed, $c_s = c/\sqrt{3(1+R)}$, depends on the ratio of baryon to photon density, with $R = 3\rho_b/4\rho_\gamma$. The sound horizon is sensitive to the physics of the early universe, including the pre-recombination expansion history and the number of effective neutrino species, N_{eff} , while $D_M(z)$ and $H(z)$ at the effective redshift of the survey depend on the late-time expansion.

In some cases, only a joint constraint, for example, on $D_V(z)/r_d$, where $D_V(z) = [czD_M^2(z)/H(z)]^{1/3}$, is provided, representing an angle-averaged constraint. This can be helpful where the BAO feature is detected at lower significance and the separate line-of-sight and transverse measures are poorly constrained or have distributions with non-Gaussian tails. Whenever possible, we use the joint anisotropic $D_M(z)/r_d$ and $H(z)r_d$ constraints. Quantities like $D_V(z)/r_d$ entail a compression of information that potentially gives a false sense of agreement with other data, as discussed in Section 3.2.

2.1. Current BAO Constraints

The BAO data sets included in fits presented in this paper are listed in Table 1. For the 6dF Galaxy Survey (6dFGS) and Sloan Digital Sky Survey (SDSS) Main Galaxy Sample (MGS), we adopt a simple Gaussian likelihood for $r_d/D_V(z)$ or $D_V(z)/r_d$. Away from the peak of the likelihood, these constraints become non-Gaussian; however, the uncertainties for these measurements are large enough that the preferred model solutions never lie far from the peak in a joint fit with other data. We use the consensus BAO scale measurements

⁴ This result is taken from the *Planck* 2015 base_plikHM_TTTEEE_lowTEB_post_BAO and base_nnu_plikHM_TTTEEE_lowTEB_nnp39_BAO chains.

⁵ <http://www.sdss3.org/surveys/boos.php>

⁶ The sound horizon was referred to as r_s by Addison et al. (2013); we have adopted the r_d notation here for consistency with other work.

Table 1
BAO Measurements Used in This Work

Data Set	LSS Tracer	z_{eff}	Measurement ^a	Constraint ^a	References
6dFGS	galaxies	0.106	$r_d/D_V(z_{\text{eff}})$	0.336 ± 0.015	Beutler et al. (2011)
SDSS MGS	galaxies	0.15	$D_V(z_{\text{eff}})r_{d,\text{fid.}}/r_d$ [Mpc]	664 ± 25	Ross et al. (2015)
BOSS DR12	galaxies	0.38	$D_M(z_{\text{eff}})r_{d,\text{fid.}}/r_d$ [Mpc]	1512 ± 25	Alam et al. (2017)
			$H(z_{\text{eff}})r_d/r_{d,\text{fid.}}$ [$\text{km s}^{-1} \text{Mpc}^{-1}$]	81.2 ± 2.4	
		0.51	$D_M(z_{\text{eff}})r_{d,\text{fid.}}/r_d$ [Mpc]	1975 ± 30	
			$H(z_{\text{eff}})r_d/r_{d,\text{fid.}}$ [$\text{km s}^{-1} \text{Mpc}^{-1}$]	90.9 ± 2.3	
		0.61	$D_M(z_{\text{eff}})r_{d,\text{fid.}}/r_d$ [Mpc]	2307 ± 37	
			$H(z_{\text{eff}})r_d/r_{d,\text{fid.}}$ [$\text{km s}^{-1} \text{Mpc}^{-1}$]	99.0 ± 2.5	
BOSS DR11 Ly α	Ly α absorbers ^b	2.34	$D_A(z_{\text{eff}})/r_d$	11.28 ± 0.65	Delubac et al. (2015)
			$c/[H(z_{\text{eff}})r_d]$	9.18 ± 0.28	
BOSS DR11 QSO \times Ly α	QSO, Ly α ^b	2.36	$D_A(z_{\text{eff}})/r_d$	10.8 ± 0.4	Font-Ribera et al. (2014)
			$c/[H(z_{\text{eff}})r_d]$	9.0 ± 0.3	

Notes.

^a Note that the fiducial sound horizon, $r_{d,\text{fid.}}$, differs across different analyses. We provide constraints here only to show relative precision. For parameter fitting we use full-likelihood surfaces, including correlations across the BOSS redshift bins or between D_M and H .

^b For brevity we refer to the Ly α and QSO \times Ly α measurements collectively as Ly α .

from the BOSS Data Release 12 (DR12), including $D_M(z)/r_d$ and $H(z)r_d$ for each of the three redshift bins and the six-by-six covariance matrix described by Alam et al. (2017). We restrict our analysis to the BAO scale as it is the most robust observable from LSS surveys (e.g., Weinberg et al. 2013, and references therein), and do not consider redshift-space distortion constraints or information from the broadband correlation function. We do not include results from the WiggleZ⁷ survey, which are consistent with BOSS and partially overlap in sky coverage (Beutler et al. 2016).

BAO have been measured in the Ly α forest of BOSS quasars (QSOs), and in the cross-correlation between the QSOs and Ly α absorbers, at effective redshifts of 2.3–2.4 (Busca et al. 2013; Slosar et al. 2013; Font-Ribera et al. 2014; Delubac et al. 2015; Bautista et al. 2017). BAO measurements at these redshifts, when the dark energy contribution to the total energy budget of the universe is small, are a powerful complement to the BAO from lower-redshift galaxy surveys. The analysis methodology and systematic error treatment required to extract the Ly α BAO scale are less mature than those for the galaxy BAO and are an active field of research (e.g., Blomqvist et al. 2015). The anisotropic BAO measurements from the DR11 Ly α and QSO \times Ly α analyses are in $\sim 2.5\sigma$ tension with *Planck* predictions, assuming a standard flat Λ CDM model. This tension was reduced slightly in the DR12 Ly α BAO analysis (Bautista et al. 2017). Bautista et al. (2017) found that the shift in the DR12 Ly α constraints was predominantly due to the additional data rather than some different treatment of systematic effects.⁸ We present results using the DR11 Ly α and QSO \times Ly α constraints, and from combining the galaxy and Ly α BAO, noting that $\sim 2.5\sigma$ effects can and do arise purely from statistical fluctuations, and that there is currently no known systematic error that explains this tension.

Other BAO measurements have been reported, for example, using galaxy clusters as LSS tracers (e.g., Hong et al. 2016;

Veropalumbo et al. 2016). These results are generally less precise than the galaxy BAO, at similar redshifts, and their inclusion would not significantly affect our results. Recently, the first measurement of BAO from the extended Baryon Oscillation Spectroscopic Survey (eBOSS⁹) was reported using clustering of quasars at $0.8 \leq z \leq 2.2$ (Ata et al. 2018). BAO constraints from this redshift range are potentially a useful addition to the galaxy and Ly α BAO and upcoming, higher-precision eBOSS measurements will be interesting to include in future analyses.

2.2. Choice of CMB Data for Joint Fits

Joint fits between *Planck* and BAO have been reported extensively for a range of cosmological models in recent work (e.g., Aubourg et al. 2015; Planck Collaboration et al. 2016a; Alam et al. 2017). While *Planck* provides the most precise CMB constraints, $\sim 2.5\sigma$ tension exists between determination of some parameters from splitting the *Planck* power spectrum into multipoles $\ell < 800$ and $\ell > 800$, where the choice of 800 corresponds to a roughly even division of overall constraining power (Addison et al. 2016). In the full Λ CDM model space, the tension is not significant (1.8σ for the assumptions used by Addison et al. 2016; see also Planck Collaboration et al. 2017). Current low-redshift cosmological observations do not provide strong constraints across the full Λ CDM parameter space, but they do provide independent and precise constraints on a subset of parameters, including H_0 , Ω_m , and σ_8 . These parameters are therefore of particular interest when it comes to assessing the performance of the Λ CDM model and testing for alternatives. Given the moderate internal *Planck* tension in these parameters, it is informative to consider other CMB measurements to help understand the extent to which conclusions are driven by *Planck* data, or are independent of *Planck*. In this work we therefore also include results from the final *WMAP* 9-year analysis (Bennett et al. 2013; Hinshaw et al. 2013), the Atacama Cosmology Telescope Polarimeter (ACTPol; Sherwin et al. 2017; Thornton et al. 2016; Louis et al. 2017) two-season survey, covering 548 deg², and the 2500 deg² South Pole

⁷ <http://wiggles.swin.edu.au/site/>

⁸ The DR12 QSO \times Ly α analysis, released while this work was in review, produced results consistent with DR11, in tension with *Planck* predictions at the 2.3σ level (du Mas des Bourboux et al. 2017).

⁹ <http://www.sdss.org/surveys/eboss/>

Table 2

Constraints on H_0 in the Λ CDM Model from the CMB Alone and from Combining CMB with BAO data, with the Significance of the Difference from the Distance Ladder Measurement (73.24 ± 1.74 ; Riess et al. 2016) in Parentheses, Assuming Uncorrelated Gaussian Errors (All Values Are in $\text{km s}^{-1} \text{Mpc}^{-1}$)

CMB Data Set	Large-scale Likelihood ^a	Power Spectrum Likelihoods ^b	H_0 (CMB-only)	BAO data ^c	H_0 (CMB+BAO)
WMAP 9-year	WMAP	TT, TE, EE	69.68 ± 2.17 (1.3 σ)	gal+Ly α	68.30 ± 0.72 (2.6 σ)
	"	"	"	gal	68.19 ± 0.72 (2.7 σ)
	"	"	"	Ly α	71.01 ± 2.10 (0.8 σ)
ACTPol Two-Season	$\tau = 0.07 \pm 0.02$	TT, TE, EE, $\phi\phi$	67.12 ± 2.67 (1.9 σ)	gal+Ly α	67.23 ± 0.80 (3.1 σ)
	"	"	"	gal	66.94 ± 0.77 (3.3 σ)
	"	"	"	Ly α	69.59 ± 2.61 (1.3 σ)
	"	TT, TE, EE	67.60 ± 3.56 (1.4 σ)	gal+Ly α	67.29 ± 0.83 (3.1 σ)
	$\tau = 0.055 \pm 0.009$	TT, TE, EE, $\phi\phi$	66.55 ± 2.59 (2.1 σ)	gal+Ly α	67.21 ± 0.83 (3.1 σ)
SPT-SZ	$\tau = 0.07 \pm 0.02$	TT, $\phi\phi$	71.38 ± 3.09 (0.5 σ)	gal+Ly α	68.52 ± 0.90 (2.4 σ)
	"	"	"	gal	68.25 ± 0.91 (2.5 σ)
	"	"	"	Ly α	73.74 ± 2.84 (0.2 σ)
	"	TT	73.20 ± 3.54 (0.0 σ)	gal+Ly α	68.49 ± 0.92 (2.4 σ)
	$\tau = 0.055 \pm 0.009$	TT, $\phi\phi$	70.67 ± 3.06 (0.7 σ)	gal+Ly α	68.46 ± 0.88 (2.5 σ)
Planck	lowTEB ^d	plikHM_TT 2015, $\phi\phi$	67.86 ± 0.92 (2.7 σ)	gal+Ly α	68.06 ± 0.56 (2.8 σ)
	"	"	"	gal	67.95 ± 0.54 (2.9 σ)
	"	"	"	Ly α	68.17 ± 0.93 (2.6 σ)
	lowTEB	plikHM_TT 2015	67.81 ± 0.92 (2.8 σ)	gal+Ly α	67.97 ± 0.56 (2.9 σ)
	$\tau = 0.055 \pm 0.009$, lowl ^e	plikHM_TT 2015	66.88 ± 0.91 (3.2 σ)	gal+Ly α	67.72 ± 0.54 (3.0 σ)
	$\tau = 0.055 \pm 0.009$, lowl	plikHM_TTEEE 2015	66.93 ± 0.62 (3.4 σ)	gal+Ly α	67.53 ± 0.45 (3.2 σ)
	$\tau = 0.07 \pm 0.02$, lowl	plikHM_TT $\ell < 800$	70.08 ± 1.96 (1.2 σ)	gal+Ly α	68.34 ± 0.67 (2.6 σ)
	$\tau = 0.055 \pm 0.009$, lowl	plikHM_TT $\ell < 800$	69.78 ± 1.86 (1.4 σ)	gal+Ly α	68.29 ± 0.66 (2.7 σ)
	$\tau = 0.07 \pm 0.02$	plikHM_TT $\ell > 800$	65.12 ± 1.45 (3.6 σ)	gal+Ly α	67.91 ± 0.66 (2.9 σ)
	$\tau = 0.055 \pm 0.009$	plikHM_TT $\ell > 800$	64.30 ± 1.31 (4.1 σ)	gal+Ly α	67.55 ± 0.62 (3.1 σ)

Notes.

^a Pixel-based and other likelihoods used at multipoles $\ell \lesssim 30$. For some fits, particularly with the ACTPol and SPT experiments that do not probe these scales, we indicate the Gaussian prior adopted on τ instead.

^b Temperature, E-mode polarization, temperature-polarization cross-spectrum, and lensing potential power spectra are denoted TT, EE, TE, and $\phi\phi$, respectively.

^c “Gal” refers to galaxy BAO; “Ly α ” refers to Ly α forest and QSO \times Ly α BAO (see Table 1).

^d lowTEB is the combined temperature-plus-polarization *Planck* likelihood for $\ell < 30$.

^e Since the *Planck* Collaboration et al. (2017) low-multipole polarization likelihood is not publicly available, we approximate its inclusion with a prior $\tau = 0.055 \pm 0.009$, which produces constraints in very good agreement with their Table 8. lowl is the *Planck* temperature-only likelihood for $\ell < 30$ (no polarization).

Telescope Sunyaev–Zel’dovich survey (SPT-SZ; Carlstrom et al. 2011; van Engelen et al. 2012; Story et al. 2013).

3. Results

3.1. Combining BAO and CMB Anisotropy Measurements

In Table 2 we show H_0 constraints within the Λ CDM model from CMB data sets with and without the inclusion of the BAO data. ACTPol and SPT use WMAP or *Planck* data only to provide an absolute calibration, that is, a single scale-independent multiplicative rescaling of the measured power spectrum. Since these experiments do not measure τ , we adopt a Gaussian prior, either the same broader $\tau = 0.07 \pm 0.02$ prior used by *Planck* Collaboration et al. (2016c) and Addison et al. (2016), or the $\tau = 0.055 \pm 0.009$ constraint from the latest *Planck* HFI low- ℓ polarization determination (*Planck* Collaboration Int. XLVI 2016). Here and throughout this paper we quote the mean and standard deviation from MCMC runs using the CosmoMC¹⁰ package (Lewis & Bridle 2002), with convergence criterion $R - 1 < 0.01$ (Gelman & Rubin 1992). Since we are not investigating foreground modeling in this

work, we use foreground-marginalized CMB likelihood codes for ACTPol and SPT (Calabrese et al. 2013; Dunkley et al. 2013). Uncertainties in foreground and other nuisance parameters propagate to cosmological parameters through an increase in power spectrum uncertainties in these codes. In the *Planck* rows of Table 2 we include the exact name of the likelihood file for clarity since a range of likelihoods have been provided by the *Planck* collaboration. These likelihoods include *Planck* foreground and nuisance parameters as described by *Planck* Collaboration et al. (2016c). We show results with and without CMB lensing power spectra (denoted “ $\phi\phi$ ” in the third column of Table 2), noting that the lensing measurements have a moderate effect on some of the CMB-only constraints but a reduced impact when the BAO are included. In the last four rows of Table 2 we also list constraints from splitting the *Planck* temperature power spectrum at $\ell = 800$ (Addison et al. 2016), as mentioned in Section 2.2 and discussed further in Section 4.

Adding galaxy BAO to any of the CMB measurements listed in Table 2 substantially tightens the H_0 prediction, by more than a factor of three in the case of ACTPol or SPT. While there is still scatter in the CMB + galaxy BAO H_0 values, the spread is substantially reduced compared to the CMB-only column. The ACTPol+BAO and SPT+BAO combinations

¹⁰ <http://cosmologist.info/cosmomc/>

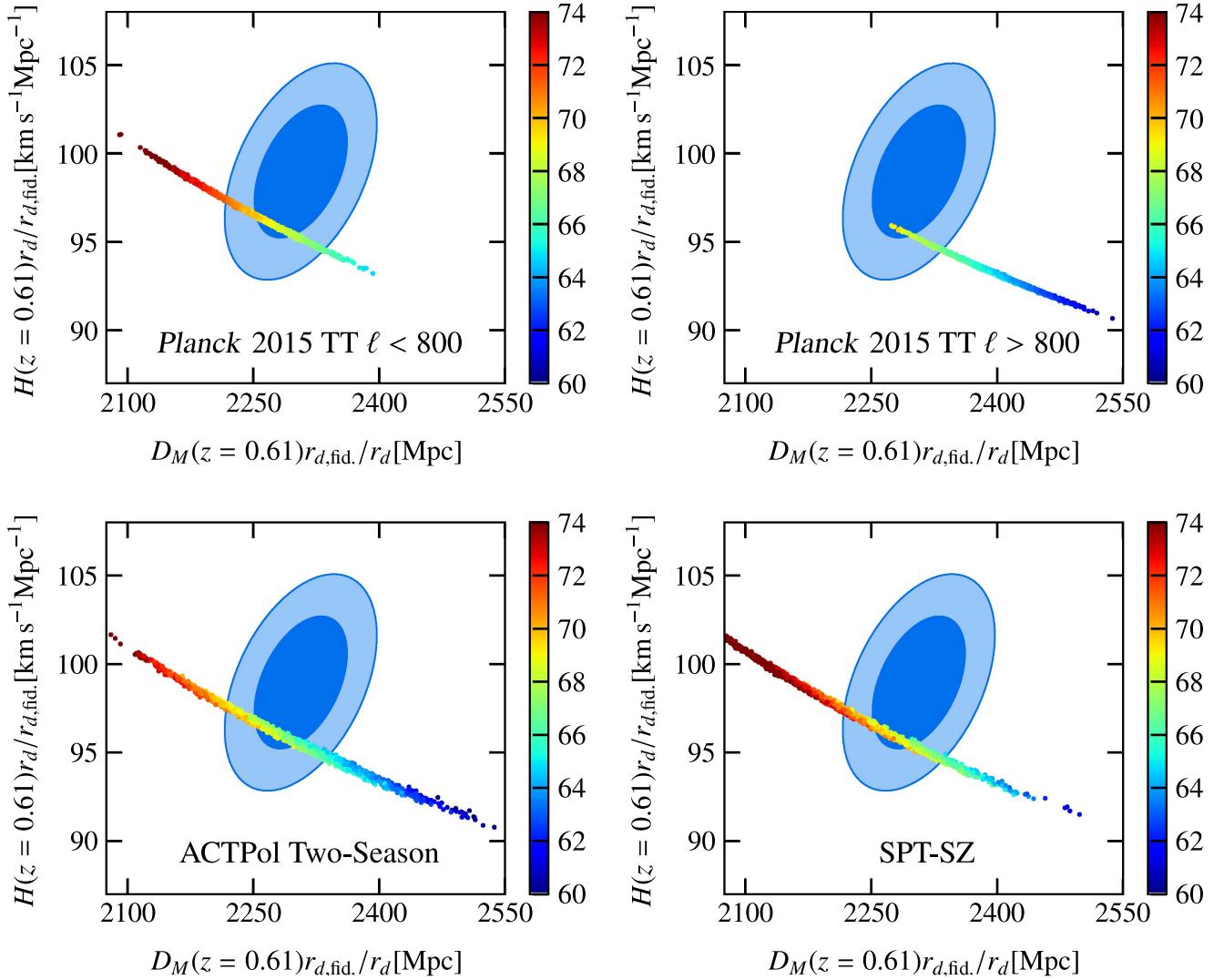


Figure 1. Including BAO data substantially tightens CMB constraints on H_0 . The observables corresponding to the transverse and line-of-sight BAO scale, $D_M r_{d,\text{fid}}/r_d$, and $H r_{d,\text{fid}}/r_d$, (Section 2 and Table 1), are shown for redshift $z = 0.61$. The blue shaded contours are the measurements from the final BOSS DR12 analysis (Alam et al. 2017). The different panels contain predictions from different, essentially independent CMB measurements, assuming a flat Λ CDM model, with MCMC samples color-coded by H_0 in $\text{km s}^{-1} \text{Mpc}^{-1}$. The same $\tau = 0.07 \pm 0.02$ prior is used in each case. The addition of BAO tightens the H_0 constraint by more than a factor of three in the case of ACTPol or SPT data (Table 2). When combined with *any* current CMB data set the galaxy BAO disfavors the values of H_0 preferred by the distance ladder ($73.24 \pm 1.74 \text{ km s}^{-1} \text{Mpc}^{-1}$; Riess et al. 2016) at moderate to high significance. The lower values preferred by the high-multipole *Planck* data (the constraint from the samples shown in the top right panel is $65.12 \pm 1.45 \text{ km s}^{-1} \text{Mpc}^{-1}$) are also disfavored.

produce H_0 constraints of comparable precision to *Planck* alone. The synergy between the galaxy BAO and CMB measurements for Λ CDM is illustrated in Figure 1 using the BOSS DR12 anisotropic BAO measurements at $z_{\text{eff}} = 0.61$ as an example. The predictions from the CMB are shown with MCMC samples color-coded by H_0 , which vary fairly monotonically along the degeneracy line set by the angular acoustic scale, corresponding to the peak spacing in the CMB power spectrum. The MCMC samples shown are drawn from the full chains, and include points from the tails of the distributions in addition to high-likelihood samples. The shaded blue contours correspond to the BOSS measurements, which are precise enough to substantially reduce the range of H_0 values allowed by breaking CMB degeneracies. The mixing of colors visible in the ACTPol and SPT panels reflects additional degeneracy between H_0 and other parameters arising from the more limited range of angular scales provided by these data.

In conjunction with the CMB, and in the context of Λ CDM, the BAO values have the effect of disfavoring both the higher values of H_0 preferred by the distance ladder, and the lower values preferred by the *Planck* damping tail at $\ell > 800$. If we exclude *Planck*, the CMB + BAO values lie $2.4\text{--}3.1\sigma$ from the R16 measurement, depending on the choice of CMB data set. While this trend has been reported before using *WMAP* data (Bernal et al. 2016; Planck Collaboration et al. 2016a), here we show that the measurements of the damping tail from ACTPol and SPT produce the same effect even without information from the larger scales measured by the satellite experiments. The fact that combining ACTPol and BAO data produces an H_0 value $> 3\sigma$ lower than R16 provides strong evidence that the H_0 discrepancy cannot be explained solely by a systematic specific to the *Planck* data. On the other hand, using the difference-of-covariance method described in Section 4.1 of Planck Collaboration et al. (2016a), the shift in H_0 from adding the BAO to the $\ell > 800$ *Planck* temperature power spectrum is

larger than expected at the 2.2σ and 2.8σ level for the $\tau = 0.07 \pm 0.02$ and 0.055 ± 0.009 priors, respectively.

The CMB + Ly α BAO fits yield higher values of H_0 than the CMB alone, without significantly smaller uncertainties. This reflects the tension between the CMB and Ly α BAO discussed in earlier work (e.g., Delubac et al. 2015; Planck Collaboration et al. 2016a). In a joint fit with all the BAO data, the Ly α measurements lack the constraining power to overcome the galaxy BAO, and consequently our results are fairly insensitive to whether the Ly α are included along with the galaxy BAO or not. The interaction between the galaxy and Ly α BAO constraints is discussed further in Section 3.3.

We note that the SPT values in Table 2 differ from the value of $75.0 \pm 3.5 \text{ km s}^{-1} \text{ Mpc}^{-1}$ quoted in Table 3 of the original SPT analysis by Story et al. (2013). This difference is driven by three effects: (i) the inclusion of the SPT lensing $\phi\phi$ power spectrum measurement from van Engelen et al. (2012) in some of our fits; (ii) the difference in τ prior; we used 0.07 ± 0.02 or 0.055 ± 0.009 , while Story et al. (2013) used 0.088 ± 0.015 ; and (iii) different CosmoMC versions or fitting options, including the fact that we set the total neutrino mass to 0.06 eV in our fits, while Story et al. (2013) assumed massless neutrinos, which leads to a $\sim 0.2\sigma$ shift in H_0 . We have verified that if we use the Story et al. (2013) assumptions, we reproduce their 75.0 ± 3.5 constraint. Aylor et al. (2017) recently derived parameters from SPT with an updated *Planck*-based calibration and improved likelihood, however, the shift they report in H_0 is small and would not meaningfully affect our results.

3.2. Angle-averaged versus Anisotropic BAO

Bennett et al. (2014; hereafter B14) used pre-*Planck* CMB data along with BAO measurements available at the time (6dFGS, BOSS DR11, including the Ly α but not QSO \times Ly α cross-correlation; we refer to these data as BAO14) to constrain

$$H_0 = 69.3 \pm 0.7 \text{ km s}^{-1} \text{ Mpc}^{-1} \quad (WMAP + ACT + SPT + BAO14). \quad (2)$$

This value is noticeably higher than the CMB+BAO values reported in Table 2. To make a more direct comparison we performed an updated fit using *WMAP*, ACTPol, SPT, and the latest BAO data, and find

$$H_0 = 68.34 \pm 0.61 \text{ km s}^{-1} \text{ Mpc}^{-1} \quad (WMAP + ACTPol + SPT + BAO). \quad (3)$$

The difference in these values appears large given the overlap in data sets used, so we investigated this difference in detail. We found that the downward shift in our current fits is due to a combination of several effects:

- (i) The biggest difference comes from using the transverse and line-of-sight BOSS BAO scale measurements now available separately rather than the angle-averaged $D_V(z)/r_d$ used in B14. Using the BOSS DR11 CMASS anisotropic BAO instead of the BOSS DR11 CMASS angle-averaged BAO shifts the *WMAP*+ACT+SPT+BAO14 H_0 constraint downwards by $0.61 \text{ km s}^{-1} \text{ Mpc}^{-1}$, a shift comparable to the total uncertainty. This is discussed in more detail below.
- (ii) A smaller shift of around $0.2 \text{ km s}^{-1} \text{ Mpc}^{-1}$ is due to different likelihood codes. We find $H_0 = 69.07 \pm 0.70 \text{ km s}^{-1} \text{ Mpc}^{-1}$ using *WMAP*9+ACT+SPT+BAO14.

Our results were obtained with the November 2016 versions of CAMB¹¹ and CosmoMC, while a different MCMC code was used in B14. Furthermore, our implementation of the DR11 Ly α BAO constraint uses the χ^2 look-up tables provided by BOSS,¹² whereas B14 constructed a likelihood directly from values reported by Delubac et al. (2015).

- (iii) The ACTPol data have a stronger downward pull on H_0 than ACT. Both ACT and ACTPol prefer a lower H_0 value than *WMAP* alone (Sievers et al. 2013; Louis et al. 2017). The SPT data prefer a higher H_0 value than *WMAP*, and this preference wins out in the combination with ACT. With ACTPol, however, the downward pull is stronger, and the resulting constraint shifts downward from 69.98 ± 1.58 (*WMAP*9+ACT+SPT) to $69.08 \pm 1.37 \text{ km s}^{-1} \text{ Mpc}^{-1}$ (*WMAP*+ACTPol+SPT). In combination with the BAO the impact of using ACTPol instead of ACT is subdominant to the choice of BAO constraints.
- (iv) The SDSS MGS BAO constraint at $z_{\text{eff}} = 0.15$ was not used by B14. While the MGS measurement has lower precision than BOSS (4% compared to around 1%), it also has a stronger preference for lower H_0 in conjunction with the CMB data.

Why does the choice of anisotropic or angle-averaged BOSS CMASS BAO make such a large difference given the same galaxy sample is used for each? In the flat Λ CDM model, all the information from any BAO measurement is contained in contours in the two-dimensional $\Omega_m - H_0 r_d$ space (Addison et al. 2013). The relative late-time expansion history is determined by Ω_m , with Ω_Λ determined implicitly by the flatness constraint. The impact of radiation on the late-time expansion is small enough compared to the precision of current BAO measurements that uncertainties in the CMB temperature, which constrains the physical density $\Omega_r h^2$, or in converting to the fractional density, Ω_r , can be neglected. The combination $H_0 r_d$ provides an overall normalization factor and reflects the fact that the absolute length of the sound horizon, and a change in the normalization of the expansion rate, are completely degenerate when only fitting to measurements of the BAO scale.

The upper left and lower left panels of Figure 2 shows constraints in the $\Omega_m - H_0 r_d$ plane for the DR11 BOSS CMASS sample at $z_{\text{eff}} = 0.57$ (Anderson et al. 2014). We show the transverse (D_M/r_d) and line-of-sight ($H r_d$) contours separately, as well as the contour from combining both, and the angle-averaged $D_V(z)/r_d$ contour. While there is substantial overlap between the combined anisotropic contour and the $D_V(z)/r_d$ contour, a portion of the parameter space is allowed by $D_V(z)/r_d$ but ruled out by the combined anisotropic measurements. This portion is relevant when the BAO and CMB are combined, as shown in the upper right and lower right panels of Figure 2, with the anisotropic $D_M(z)/r_d + H(z)r_d$ constraint pulling down more strongly on $H_0 r_d$, and hence H_0 , since H_0 and r_d are only partially degenerate in the CMB. The same effect is apparent in Figure 8 of Cuesta et al. (2016).

We conclude that the shift in H_0 from using the angle-averaged $D_V(z)/r_d$ instead of the full anisotropic BAO information is not caused by an inconsistency in the BAO measurements, but instead due to the compression of

¹¹ <http://camb.info/>

¹² <http://darkmatter.ps.uci.edu/baofit/>

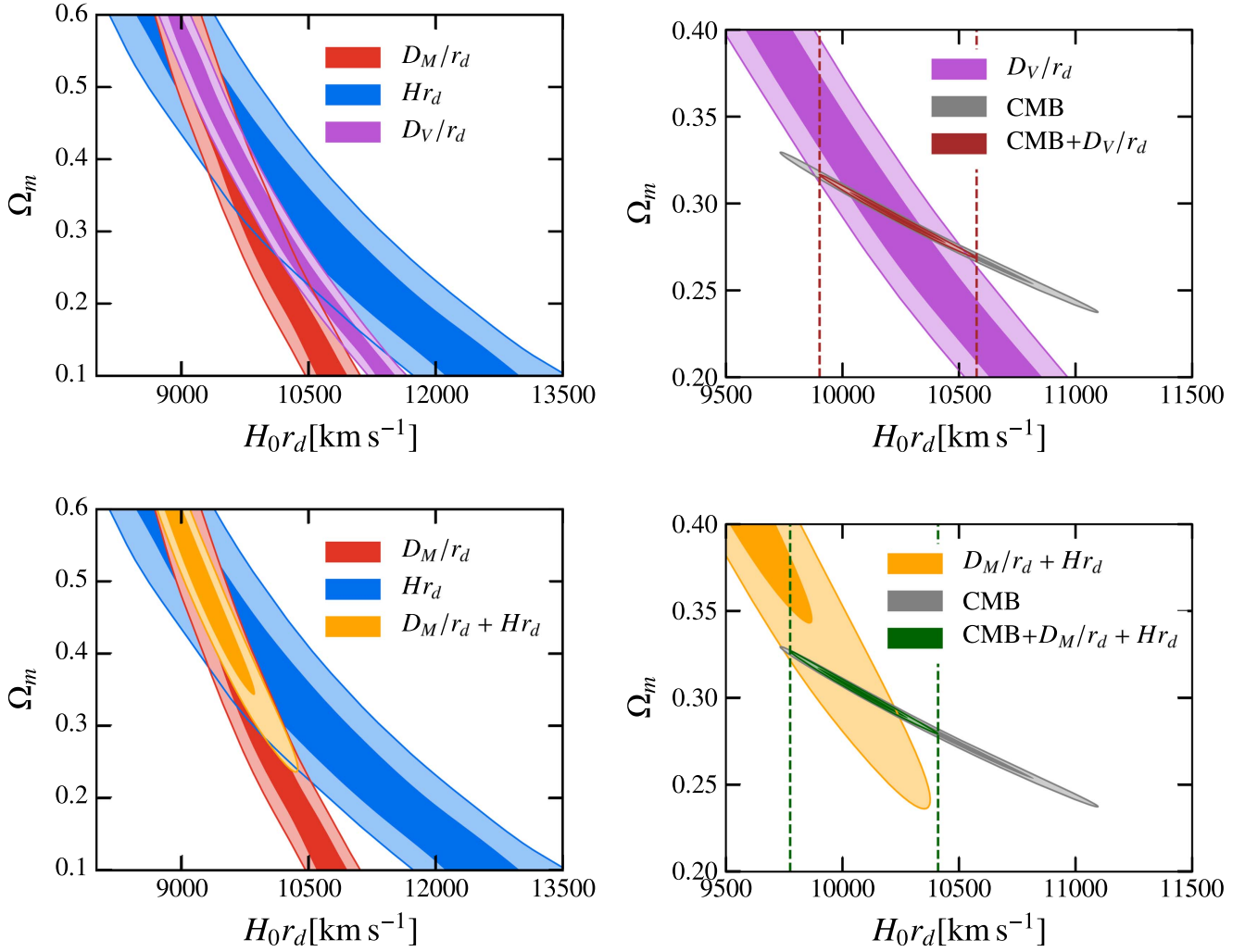


Figure 2. Use of the angle-averaged BAO constraint, $D_V(z)/r_d$, instead of the full anisotropic information, $D_M(z)/r_d$ plus $H(z)r_d$, can impact determination of H_0 from combined CMB+BAO fits. The upper left panel shows constraints from the same BOSS CMASS DR11 galaxy sample at $z_{\text{eff}} = 0.57$ (Anderson et al. 2014) but different BAO measures—transverse (D_M/r_d), line of sight (Hr_d), and angle-averaged (D_V/r_d , see Section 2.1). The lower left panel shows the anisotropic constraint from combining $D_M(z)/r_d$ and $H(z)r_d$. While there is significant overlap between the angle-averaged and anisotropic contours, the angle-averaged contour extends to lower values of Ω_m , which are not allowed by the anisotropic constraint. The upper right and lower right panels show the effect of adding the BAO information to CMB data (we show the same data sets used by Bennett et al. 2014, WMAP+ACT+SPT). The use of the angle-averaged $D_V(z)/r_d$ constraint diminishes the downward pull on $H_0 r_d$, and also H_0 , from the BAO. The vertical dashed lines correspond to the bounds of the contours containing 95% of the CMB+BAO MCMC samples.

information inherent to $D_V(z)/r_d$. It is therefore preferable to use the anisotropic constraints where possible.

3.3. Constraints from the BAO Scale Alone

We now consider constraints from the BAO data without the strong additional constraining power of the CMB anisotropy measurements. As discussed above, in the flat Λ CDM model, BAO measurements provide contours in the $\Omega_m - H_0 r_d$ plane. Combining the galaxy and Ly α BAO provides a tight constraint on Ω_m from the late-time expansion history, even when marginalizing over the normalization $H_0 r_d$. For the BAO listed in Table 1 we find constraints of

$$\begin{aligned} \Omega_m &= 0.292 \pm 0.020 \\ H_0 r_d &= (10119 \pm 138) \text{ km s}^{-1}. \end{aligned} \quad (4)$$

The left panel of Figure 3 shows constraints from the galaxy and Ly α BAO in the $\Omega_m - H_0 r_d$ plane. The orientation of these

contours can be approximately understood from considering the redshift dependence of $H(z)$. Similar arguments hold for $D_A(z)$. At the Ly α BAO redshifts the universe is matter-dominated, and $H(z) \simeq H_0 \Omega_m^{1/2} (1+z)^{3/2}$, so that $H(z)r_d$ constraints produce contours along the direction with $H_0 r_d \cdot \Omega_m^{1/2}$ roughly constant. At lower redshifts, where dark energy becomes dominant, $H(z)$ depends less strongly on Ω_m , leading to the galaxy BAO contour being oriented more along the direction of the y-axis in Figure 3.¹³ There is little overlap between the galaxy and Ly α contours. To quantify this difference, we consider the test described in Section 4.1 of Hou et al. (2014). We calculate $\Delta\chi^2 = \chi_{X+Y}^2 - \chi_X^2 - \chi_Y^2$, where in this case X and Y are the galaxy and Ly α BAO data, respectively, χ_{X+Y}^2 denotes the best-fit χ^2 from the joint fit, and χ_X^2 and χ_Y^2 are the best-fit χ^2 from the fits to just the galaxy or

¹³ If BAO measurements at $z = 0$ were possible, they would produce exactly vertical contours in Figure 3.

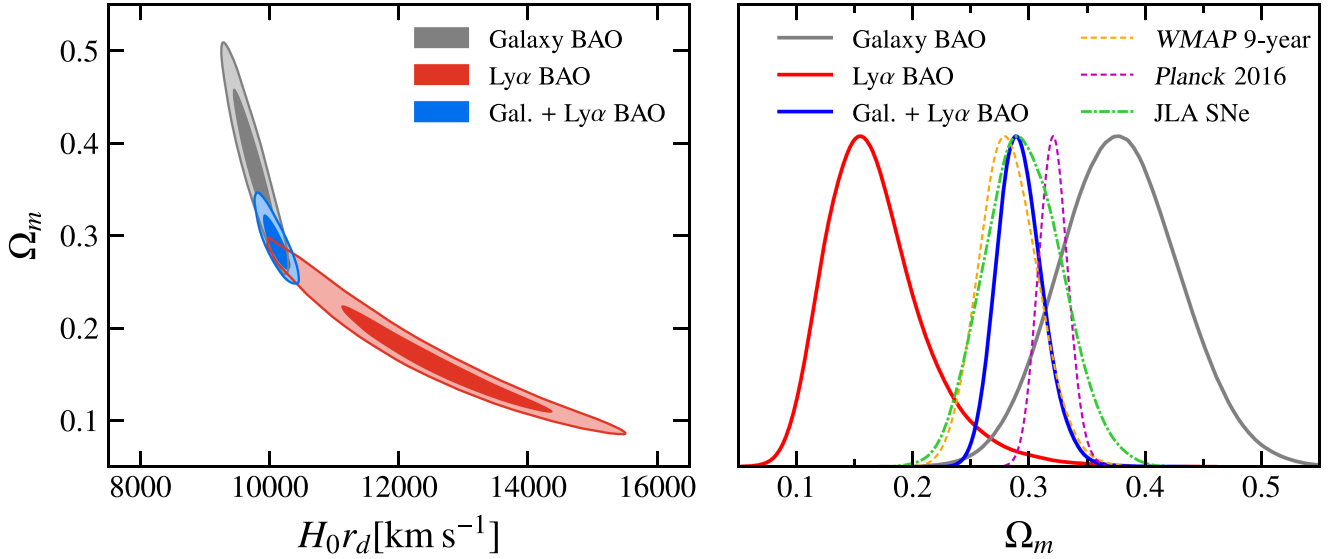


Figure 3. Left: comparison of BAO-only constraints in the flat Λ CDM model. Contours containing 68 and 95% of MCMC samples are shown for galaxy ($z_{\text{eff}} \leq 0.61$) and Ly α forest ($z_{\text{eff}} \geq 2.3$) BAO separately and in a joint fit using the BAO data listed in Table 1. In flat Λ CDM the late-time expansion rate is determined only by Ω_m , with $H_0 r_d$ acting as an overall expansion normalization. Right: comparison of Ω_m constraints from BAO, CMB, and SNe measurements. The SNe constraint is from the “joint light-curve analysis” (JLA) presented by Betoule et al. (2014). While the combined BAO fit produces a tight constraint $\Omega_m = 0.293 \pm 0.020$, in agreement with the CMB and SNe determinations, there is a 2.4σ tension between the galaxy and Ly α BAO, which individually prefer higher and lower values of Ω_m , respectively.

Table 3

Λ CDM Constraints from the BAO+D/H Fits, Using either the Theoretical or Empirical $d(p, \gamma)^3\text{He}$ Reaction Rate, with CMB Anisotropy Constraints from *WMAP* and *Planck* Included for Comparison

Parameter	BAO+D/H (theoretical)	BAO+D/H (empirical)	<i>WMAP</i> 9-year	<i>Planck</i> 2016
$100\Omega_b h^2$	2.156 ± 0.020	2.257 ± 0.034	2.265 ± 0.049	2.215 ± 0.021
$100\Omega_c h^2$	10.94 ± 1.20	11.19 ± 1.29	11.37 ± 0.46	12.07 ± 0.21
$100\theta_{\text{MC}}$	1.0292 ± 0.0168	1.0320 ± 0.0173	1.04025 ± 0.00223	1.04076 ± 0.00047
H_0 [km s $^{-1}$ Mpc $^{-1}$]	66.98 ± 1.18	67.81 ± 1.25	69.68 ± 2.17	66.89 ± 0.90
Ω_m	0.293 ± 0.019	0.293 ± 0.020	0.283 ± 0.026	0.321 ± 0.013
r_d [Mpc]	151.6 ± 3.4	149.2 ± 3.6	148.49 ± 1.23	147.16 ± 0.48

just the Ly α data. For Gaussian-distributed data,¹⁴ if X and Y are independent and Λ CDM is the correct model, then $\Delta\chi^2$ is drawn from a χ^2 distribution with $N_{\Delta\chi^2} = N_{X+Y} - N_X - N_Y$ degrees of freedom (dof). We find

$$\begin{aligned}
 \chi_{\text{gal}}^2 &= 2.98 & N_{\text{gal}} &= 8-2 = 6 \\
 \chi_{\text{Ly}\alpha}^2 &= 0.92 & N_{\text{Ly}\alpha} &= 4-2 = 2 \\
 \chi_{\text{gal+Ly}\alpha}^2 &= 13.63 & N_{\text{gal+Ly}\alpha} &= 12-2 = 10 \\
 \Delta\chi^2 &= 9.73 & N_{\Delta\chi^2} &= 10-6-2 = 2.
 \end{aligned}$$

The probability of exceeding (PTE) for $\chi^2 = 9.73$ with $N_{\text{dof}} = 2$ is 7.71×10^{-3} , which corresponds to a 2.4σ disagreement. This is comparable to the 2.5σ tension reported between the Ly α BAO and *Planck* measurements by Delubac et al. (2015). As discussed by Aubourg et al. (2015), modifying the cosmological model to improve three-way agreement

between CMB, galaxy BAO, and Ly α BAO appears difficult. Here, we note that the combined contour in Figure 3 lies at the intersection of the main degeneracy directions determined by the redshift coverage of the galaxy and Ly α measurements. If future data shift the galaxy or Ly α BAO constraints *along* these degeneracy lines (as opposed to perpendicular to them) the main result would be to change the quality of the combined fit rather than changing the parameter values. We further note that the matter density reported in (4) is in agreement with the value of 0.295 ± 0.034 from a joint analysis of type Ia SNe from several surveys covering $0 < z < 1$, completely independent of LSS clustering (Betoule et al. 2014). This is illustrated in the right panel of Figure 3, which shows a comparison of BAO, *WMAP* 9-year, *Planck* 2016,¹⁵ and SNe constraints on Ω_m for the flat Λ CDM model.

¹⁴ This is a reasonable approximation when the Ly α and QSO \times Ly α BAO are combined (Delubac et al. 2015).

¹⁵ We refer to the combination of the 2015 TT constraints with updated $\tau = 0.055 \pm 0.009$ prior from Planck Collaboration et al. (2017) as “*Planck* 2016.”

3.4. Constraining H_0 with BAO plus Deuterium Abundance in Λ CDM

Obtaining a constraint on H_0 from the BAO requires adding information to break the $H_0 - r_d$ degeneracy. One way to do this is to add a constraint on the baryon density (e.g., Addison et al. 2013; Aubourg et al. 2015; Wang et al. 2017). We assume that the photon energy density, or, equivalently, the CMB mean temperature, is also known. The CMB temperature was measured precisely by *COBE*/FIRAS (Fixsen et al. 1996; Fixsen 2009) and we view this result as independent of the CMB anisotropy measurements performed by more recent experiments. Note that while the H_0 in the $H(z)$ in the denominator of (1) cancels in the $H_0 r_d$ product, some residual H_0 dependence still exists because the decoupling redshift and the sound speed depend on the *physical* matter and radiation densities, $\Omega_m h^2$ and $\Omega_r h^2$, respectively, while the expansion rate $H(z)$ depends on the *fractional* densities Ω_m and Ω_r .

In the BAO fit with an external baryon density prior, Ω_m performs double duty. It not only goes into determining the late-time expansion (D_M and H at the BAO survey redshifts) but also controls the expansion history in the early universe prior to baryons decoupling from photons, since the photon and neutrino properties (with $N_{\text{eff}} = 3.046$) are held fixed. As well as providing an indirect H_0 constraint, the BAO+ $\Omega_b h^2$ fit also serves as something of a self-consistency test of early and late-time expansion.

The most precise constraints on $\Omega_b h^2$ independent of the CMB power spectrum come from estimates of the primordial deuterium abundance. In standard Big Bang nucleosynthesis (BBN), the abundance of light nuclei is determined by a single parameter, the baryon-to-photon ratio η (see recent review by Cyburt et al. 2016, and references therein). Taking the photon number density as fixed from the CMB temperature, a measurement of the primordial deuterium abundance in conjunction with knowledge of BBN physics provides a constraint on $\Omega_b h^2$. Precise estimates of the primordial deuterium abundance have been made in recent years using extremely metal-poor damped Ly α (DLA) systems along sight lines to high-redshift quasars (e.g., Pettini & Cooke 2012; Cooke et al. 2014, 2016; Riemer-Sørensen et al. 2017). Cooke et al. (2016; hereafter C16) report

$$10^5 \text{D}_I/\text{H}_I = 2.547 \pm 0.033 \quad (5)$$

by combining six such systems. The $d(p, \gamma)^3\text{He}$ reaction rate plays a key role in the conversion from D/H to $\Omega_b h^2$. Using the theoretical calculation for this rate from Marcucci et al. (2016), C16 find

$$100\Omega_b h^2 = 2.156 \pm 0.020 \quad (\text{D/H, theoretical rate}), \quad (6)$$

which is $>2\sigma$ lower than the *Planck* value (assuming a standard Λ CDM model throughout). Using instead an empirically derived $d(p, \gamma)^3\text{He}$ rate, C16 find

$$100\Omega_b h^2 = 2.260 \pm 0.034 \quad (\text{D/H, empirical rate}), \quad (7)$$

which has a larger uncertainty but is in better agreement with CMB-derived values. We performed fits to the galaxy-plus-Ly α BAO data with the addition of each of the Gaussian priors on $\Omega_b h^2$ in (6) and (7) in turn. We show parameter constraints

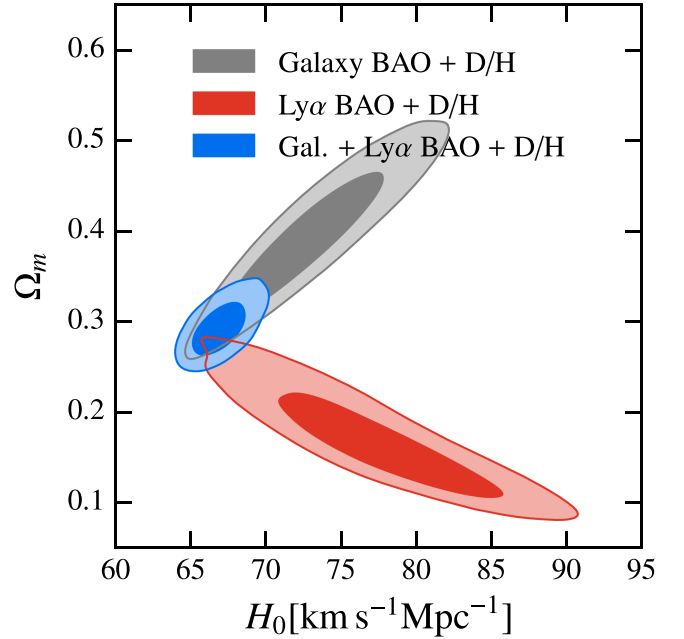


Figure 4. Adding an estimate of the baryon density, $\Omega_b h^2$, in this case from deuterium abundance (D/H) measurements, breaks the BAO $H_0 - r_d$ degeneracy in Λ CDM. The same contours are shown as in Figure 3, with the addition of a Gaussian prior $100\Omega_b h^2 = 2.156 \pm 0.020$ (Cooke et al. 2016). In contrast to Figure 3, here Ω_m determines both the early time expansion, including the absolute sound horizon, r_d , as well as the late-time expansion history. The radiation density is fixed from *COBE*/FIRAS CMB mean temperature measurements. The combined BAO+D/H constraint, $H_0 = 66.98 \pm 1.18 \text{ km s}^{-1} \text{ Mpc}^{-1}$ is 3.0σ lower than the Riess et al. (2016) distance ladder determination and is independent of CMB anisotropy data.

in Table 3, including the *WMAP* 9-year and *Planck* 2016 CMB anisotropy constraints for comparison.

In the BAO+D/H fits, $\Omega_b h^2$ is driven solely by the D/H prior, as expected, and Ω_m matches the BAO-only value. While the choice of the $d(p, \gamma)^3\text{He}$ reaction rate significantly impacts the value of $\Omega_b h^2$, it has a reduced impact on the inferred H_0 , because r_d only depends weakly on $\Omega_b h^2$ (Eisenstein & Hu 1998; Addison et al. 2013). Specifically, replacing the theoretical rate with the empirical one shifts the center of the $\Omega_b h^2$ distribution by 5.2 times the original uncertainty, but shifts the H_0 distribution by only 0.7 times the original uncertainty. Our BAO+D/H results for H_0 are more robust to the choice of rate than one might expect from the $\Omega_b h^2$ difference.

The H_0 values listed in Table 3 from the BAO+D/H fits have uncertainties of around 1.8% and are 3.0 and 2.5σ lower than the R16 distance ladder value of $73.24 \pm 1.74 \text{ km s}^{-1} \text{ Mpc}^{-1}$ for the theoretical and empirical $d(p, \gamma)^3\text{He}$ rates, respectively. The combination of precise BAO and D/H measurements enables determinations of H_0 within the context of the flat Λ CDM model that are almost 50% tighter than the distance ladder measurement, and lower at moderate to strong significance. We emphasize that these constraints are completely independent of CMB anisotropy measurements.

Constraints in the $\Omega_m - H_0$ plane for the BAO+D/H fits with the theoretical $d(p, \gamma)^3\text{He}$ rate are shown in Figure 4. We show results from the galaxy and Ly α BAO separately and together, as before. Tension between the galaxy and Ly α BAO is again apparent. Adding D/H to these data separately favors higher values of H_0 , and it is only when galaxy and Ly α BAO

are combined that H_0 is constrained to the values quoted in Table 3.

The direction of the Ly α BAO contour is roughly the same in the left panel of Figure 3 and in Figure 4, while that of the galaxy BAO contour changes. This behavior can be understood by considering how r_d depends on Ω_m and H_0 . For a given value of $\Omega_b h^2$, r_d depends approximately on the combination $H_0 \cdot \Omega_m^{1/2}$ (Equation (26) of Eisenstein & Hu 1998). This is the same dependence as $H(z)$ at the Ly α redshifts (Section 3.3) and is related to the fact that the universe is largely matter-dominated in both cases. The dependence of $H(z)$ on Ω_m at the galaxy BAO redshifts is weaker, and the direction of the galaxy BAO contour in Figure 4 is approximately determined by requiring $H_0 r_d$ to be roughly constant as Ω_m varies. This produces a positive correlation between H_0 and Ω_m because r_d decreases as $H_0 \Omega_m^{1/2}$ increases.

For the BAO+D/H fits, we ran CosmoMC as one would when fitting to the CMB: the fitted parameters are $\Omega_b h^2$, the physical cold dark matter density, $\Omega_c h^2$, and the angular sound horizon, θ_{MC} , and H_0 , Ω_m , and r_d are derived from these three. Since the BAO+D/H data are insensitive to the amplitude and tilt of the primordial power spectrum, and the optical depth to reionization, these other Λ CDM parameters are held fixed. Consistent results were obtained using earlier BAO and D/H data by Addison et al. (2013) and Aubourg et al. (2015). We note that Riemer-Sorensen & Sem Jønsen (2017) recently obtained a tighter constraint on D/H than we have used here by combining the DLAs used by C16 with a number of additional measurements. Using this tighter constraint would not impact our conclusions.

3.5. BAO and Light Element Abundance Constraints with Varying N_{eff}

In the Λ CDM+ N_{eff} model, there is a perfect degeneracy between $\Omega_b h^2$ and N_{eff} from D/H measurements (Figure 6 of C16). Closed contours in the $\Omega_b h^2 - N_{\text{eff}}$ plane can be obtained from combining estimates of the primordial D/H and ^4He abundance (e.g., review by Cyburt et al. 2016, and references therein). The primordial ^4He abundance is estimated from He and H emission lines in extragalactic H II regions. Obtaining accurate constraints is challenging due to dependence on environmental parameters such as temperature, electron density, and metallicity, which must be modeled. An important recent development is the use of the He I line at 10830 Å to help break modeling degeneracies (Izotov et al. 2014). The value of the primordial helium fraction reported by Izotov et al. (2014), $Y_p = 0.2551 \pm 0.0022$, is, however, significantly higher than values found in some subsequent analyses of the same H II sample using different selection criteria and fitting methodology. For example, Aver et al. (2015) found $Y_p = 0.2449 \pm 0.0040$, while Peimbert et al. (2016) found $Y_p = 0.2446 \pm 0.0029$. The different Y_p values lead to significantly different inferences for N_{eff} when used in combination with D/H or CMB power spectra measurements. Izotov et al. (2014) found evidence for additional neutrino species at 99% confidence, while, for instance, Cyburt et al. (2016) reported $N_{\text{eff}} = 2.85 \pm 0.28$, and Peimbert et al. (2016) found $N_{\text{eff}} = 2.90 \pm 0.22$, consistent with the standard model value of 3.046.

Current D/H and ^4He constraints clearly have the *precision* to weigh in significantly on the question of whether allowing $N_{\text{eff}} > 3$ is effective at resolving Λ CDM tensions. Given the

spread in Y_p values discussed above, and the impact of the choice of $d(p, \gamma)^3\text{He}$ rate when N_{eff} is allowed to vary (Section 5.2 of C16), we do not present a full set of results including BAO and light element abundance data for Λ CDM+ N_{eff} . Instead, we note that combining BAO measurements with D/H and ^4He constraints on N_{eff} that are consistent with the standard model value would produce H_0 values consistent with the values in Table 3, although with larger uncertainties, while higher values of N_{eff} would produce a higher H_0 , improving agreement with the distance ladder. The BAO measurements, only being sensitive to $H_0 r_d$, and not to H_0 or N_{eff} directly, are unable to discriminate between these possibilities.

4. Discussion

We have presented evidence for a lower H_0 value than measured by the local distance ladder that is independent of *Planck*, both from combining BAO with other CMB data sets (WMAP, ACTPol, and SPT), and from joint fits to BAO and D/H measurements, within the context of the standard Λ CDM model. In light of this analysis it is clear that the H_0 tension cannot be resolved solely through a systematic error specific to the *Planck* data. It should be noted, however, that it is not simply a case of having a “high” H_0 from the distance ladder, and a “low” H_0 from *Planck* and the joint BAO fits. The high-multipole *Planck* temperature data prefer H_0 values that are even lower than the CMB+BAO or BAO+D/H values (bottom two rows of Table 2 and top right panel of Figure 1). Restricting the *Planck* temperature power spectrum to multipoles $\ell > 800$ produces

$$H_0 = 65.12 \pm 1.45 \text{ km s}^{-1} \text{ Mpc}^{-1} \\ (\text{Planck 2015 TT } \ell > 800, \tau = 0.07 \pm 0.02), \quad (8)$$

or

$$H_0 = 64.30 \pm 1.31 \text{ km s}^{-1} \text{ Mpc}^{-1} \\ (\text{Planck 2015 TT } \ell > 800, \tau = 0.055 \pm 0.009), \quad (9)$$

depending on the choice of τ prior. These values are not only in strong tension with R16, but are in moderate tension with some of the CMB+BAO values reported in Table 2. For example, for $\tau = 0.055 \pm 0.009$, the SPT+BAO value is lower than R16 by 2.5σ , but the *Planck* $\ell > 800$ value is 2.6σ lower again than SPT+BAO. The shift in H_0 from adding the BAO to the $\ell > 800$ *Planck* constraints is also larger than expected given the improvement in precision, as discussed in Section 3.1. Some H_0 tension remains even if we do not consider the distance ladder constraints. In fact, concordance cannot be achieved through the removal of *any* single data set (e.g., BAO, CMB, distance ladder, or D/H). This is part of the reason the H_0 discrepancy is challenging to resolve: a convincing solution must simultaneously address multiple avenues of disagreement.

A wide range of fits to expanded cosmological models, with various combinations of data, have been presented in recent years to try to reconcile H_0 and other parameter tensions. Our fits in this paper have been restricted to the standard flat Λ CDM model, partly because our results for expanded models would be similar to those already presented by Planck Collaboration et al. (2016a), Alam et al. (2017), Heavens et al. (2017), and others. The BAO, CMB, and light element abundance measurements have some common dependence on the early-universe expansion history, which makes allowing freedom in,

for example, N_{eff} , seem attractive. As discussed in Section 1, varying N_{eff} does not sufficiently relieve tensions and is not statistically favored over standard Λ CDM for the current BAO, CMB, and distance ladder data. There are good prospects for tightening N_{eff} constraints through improved measurements of the high- ℓ CMB damping tail in E-mode polarization (e.g., Abazajian et al. 2015, 2016). Future BAO data, for example, from the Dark Energy Spectroscopic Instrument (DESI)¹⁶, Euclid,¹⁷ and WFIRST,¹⁸ will also provide significant improvements in precision over current measurements (for BAO+ $\Omega_b h^2$ forecasts for H_0 , see Wang et al. 2017).

5. Conclusions

We have examined the role of BAO measurements in determining H_0 . While the BAO data alone are unable to distinguish between a change in H_0 and a change in the absolute sound horizon at decoupling, r_d , this degeneracy is broken, and a precise H_0 value obtained, when BAO are combined with either CMB power spectra or deuterium abundance measurements. Overall we find convincing evidence for a lower H_0 in Λ CDM than what was obtained from the latest local distance ladder measurement ($73.24 \pm 1.74 \text{ km s}^{-1} \text{ Mpc}^{-1}$; Riess et al. 2016), even without using data from *Planck*. The motivation and results of this study are summarized as follows:

- (i) Tension at the $>3\sigma$ level exists between determinations of H_0 from the distance ladder and the CMB anisotropy measurements from *Planck*, within the context of the standard flat Λ CDM model. Other tensions also exist, for example between *Planck* data and constraints on the growth of structure from some weak lensing surveys.
- (ii) None of the cosmological modifications commonly proposed appear to provide a statistically compelling solution to these tensions, although some, such as allowing freedom in the number of effective relativistic species, N_{eff} , do reduce the H_0 disagreement.
- (iii) Combining BAO measurements with CMB power spectrum data from *WMAP*, ACTPol, or SPT, produces H_0 values that are lower than the distance ladder by $2.4\text{--}3.1\sigma$, independent of *Planck* (Table 2). The difference was less pronounced in some earlier analyses because of using the angle-averaged BOSS CMASS BAO measurement. The angle-averaged $D_V(z)/r_d$ constraint is a compression of information and allows a region of parameter space that is ruled out by the full anisotropic BAO constraints (Figure 2). Adding the BAO improves the H_0 constraint from ACTPol or SPT by more than a factor of three, making their precision comparable to the *Planck*-only results.
- (iv) Combining BAO data with primordial deuterium (D/H) abundance estimates from metal-poor DLA systems produces precise H_0 values that are lower than the distance ladder by $2.5\text{--}3.0\sigma$, depending on assumptions about the $d(p, \gamma)^3\text{He}$ reaction rate (e.g., $66.98 \pm 1.18 \text{ km s}^{-1} \text{ Mpc}^{-1}$ for the theoretical rate, see Table 3). This result is independent of any CMB anisotropy measurement and relies only on the CMB mean temperature from *COBE*/FIRAS.

- (v) The two previous results taken together indicate that it is not possible to resolve the H_0 disagreement solely through some systematic error specific to the *Planck* data set.
- (vi) The *Planck* high-multipole ($\ell > 800$) damping tail measurements prefer lower values of H_0 than the combined BAO fits, such as, for example, 65.12 ± 1.45 and $64.30 \pm 1.31 \text{ km s}^{-1} \text{ Mpc}^{-1}$, for $\tau = 0.07 \pm 0.02$ and $\tau = 0.055 \pm 0.009$, respectively. The shift in H_0 from adding the BAO to these data is larger than expected at the 2.2σ and 2.8σ levels for these τ priors. The H_0 disagreement is not as simple as the distance ladder value being “high” and other constraints coming out “low,” and cannot be resolved through the removal of any single data set.
- (vii) We note that a 2.4σ tension exists between the galaxy ($z \leq 0.61$) and Ly α ($z \geq 2.4$) BAO, as previously discussed by Aubourg et al. (2015). The BAO+D/H constraints rely on combining these measurements, thus it is important to review their consistency with future data.

In recent years new precise measurements have led to multiple tensions, particularly in H_0 , that are uncomfortably too large to be explained by statistical scatter within the context of the standard Λ CDM model. Whether this is the sign of new physics or underestimated uncertainties, or some combination of effects, remains unclear, and no straightforward explanation has yet presented itself. Near-term improvements in CMB, LSS, and distance ladder data are expected; however, continuing to scrutinize existing measurements, as we have in this work, could also prove important in moving toward an eventual resolution.

This research was supported in part by NASA grants NNX15AJ57G, NNX16AF28G, and NNX17AF34G, and JPL grant 1563692, and by the Canadian Institute for Advanced Research (CIFAR). We acknowledge the use of the Legacy Archive for Microwave Background Data Analysis (LAMBDA), part of the High Energy Astrophysics Science Archive Center (HEASARC). HEASARC/LAMBDA is a service of the Astrophysics Science Division at the NASA Goddard Space Flight Center. This work was partly based on observations obtained with *Planck* (<http://www.esa.int/Planck>), an ESA science mission with instruments and contributions directly funded by ESA Member States, NASA, and Canada. Part of this research project was conducted using computational resources at the Maryland Advanced Research Computing Center (MARCC).

The authors would like to thank Erminia Calabrese, Antony Lewis, James Rich, Adam Riess, and Ashley Ross for helpful discussions and clarifications regarding the data sets and software used in this work, and we are also grateful to Adam Riess for reading a draft of the manuscript and providing useful suggestions. We acknowledge the use of the *GetDist* plotting package.¹⁹

ORCID iDs

G. E. Addison  <https://orcid.org/0000-0002-2147-2248>
D. J. Watts  <https://orcid.org/0000-0002-5437-6121>

¹⁶ <http://desi.lbl.gov/>

¹⁷ <https://www.euclid-ec.org/>

¹⁸ <https://wfIRST.gsfc.nasa.gov/>

¹⁹ <http://getdist.readthedocs.io/en/latest/>

C. L. Bennett  <https://orcid.org/0000-0001-8839-7206>
 M. Halpern  <https://orcid.org/0000-0002-1760-0868>
 G. Hinshaw  <https://orcid.org/0000-0002-4241-8320>
 J. L. Weiland  <https://orcid.org/0000-0003-3017-3474>

References

- Abazajian, K. N., Adshead, P., Ahmed, Z., et al. 2016, arXiv:1610.02743
 Abazajian, K. N., Arnold, K., Austermann, J., et al. 2015, *APh*, **63**, 66
 Addison, G. E., Hinshaw, G., & Halpern, M. 2013, *MNRAS*, **436**, 1674
 Addison, G. E., Huang, Y., Watts, D. J., et al. 2016, *ApJ*, **818**, 132
 Alam, S., Ata, M., Bailey, S., et al. 2017, *MNRAS*, **470**, 2617
 Alsing, J., Heavens, A., & Jaffe, A. H. 2017, *MNRAS*, **466**, 3272
 Anderson, L., Aubourg, É., Bailey, S., et al. 2014, *MNRAS*, **441**, 24
 Ata, M., Baumgarten, F., Bautista, J., et al. 2018, *MNRAS*, **473**, 4773
 Aubourg, É., Bailey, S., Bautista, J. E., et al. 2015, *PhRvD*, **92**, 123516
 Aver, E., Olive, K. A., & Skillman, E. D. 2015, *JCAP*, **7**, 011
 Aylor, K., Hou, Z., Knox, L., et al. 2017, *ApJ*, **850**, 101
 Bautista, J. E., Busca, N. G., Guy, J., et al. 2017, *A&A*, **603**, A12
 Bennett, C. L., Larson, D., Weiland, J. L., et al. 2013, *ApJS*, **208**, 20
 Bennett, C. L., Larson, D., Weiland, J. L., & Hinshaw, G. 2014, *ApJ*, **794**, 135
 Bernal, J. L., Verde, L., & Riess, A. G. 2016, *JCAP*, **10**, 019
 Betoule, M., Kessler, R., Guy, J., et al. 2014, *A&A*, **568**, A22
 Beutler, F., Blake, C., Colless, M., et al. 2011, *MNRAS*, **416**, 3017
 Beutler, F., Blake, C., Koda, J., et al. 2016, *MNRAS*, **455**, 3230
 Blomqvist, M., Kirkby, D., Bautista, J. E., et al. 2015, *JCAP*, **11**, 034
 Bonvin, V., Courbin, F., Suyu, S. H., et al. 2017, *MNRAS*, **465**, 4914
 Brust, C., Cui, Y., & Sigurdson, K. 2017, *JCAP*, **8**, 020
 Busca, N. G., Delubac, T., Rich, J., et al. 2013, *A&A*, **552**, A96
 Calabrese, E., Hlozek, R. A., Battaglia, N., et al. 2013, *PhRvD*, **87**, 103012
 Cardona, W., Kunz, M., & Pettorino, V. 2017, *JCAP*, **3**, 056
 Carlstrom, J. E., Ade, P. A. R., Aird, K. A., et al. 2011, *PASP*, **123**, 568
 Cole, S., Percival, W. J., Peacock, J. A., et al. 2005, *MNRAS*, **362**, 505
 Cooke, R. J., Pettini, M., Jorgenson, R. A., Murphy, M. T., & Steidel, C. C. 2014, *ApJ*, **781**, 31
 Cooke, R. J., Pettini, M., Nollett, K. M., & Jorgenson, R. 2016, *ApJ*, **830**, 148
 Cuesta, A. J., Vargas-Magaña, M., Beutler, F., et al. 2016, *MNRAS*, **457**, 1770
 Cyburt, R. H., Fields, B. D., Olive, K. A., & Yeh, T.-H. 2016, *RvMP*, **88**, 015004
 Delubac, T., Bautista, J. E., Busca, N. G., et al. 2015, *A&A*, **574**, A59
 Dhawan, S., Jha, S. W., & Leibundgut, B. 2018, *A&A*, **609**, A72
 du Mas des Bourboux, H., Le Goff, J.-M., Blomqvist, M., et al. 2017, *A&A*, **608**, A130
 Dunkley, J., Calabrese, E., Sievers, J., et al. 2013, *JCAP*, **7**, 025
 Efsthathiou, G. 2014, *MNRAS*, **440**, 1138
 Eisenstein, D. J., & Hu, W. 1998, *ApJ*, **496**, 605
 Eisenstein, D. J., Zehavi, I., Hogg, D. W., et al. 2005, *ApJ*, **633**, 560
 Feeney, S. M., Mortlock, D. J., & Dalmasso, N. 2017, arXiv:1707.00007
 Fixsen, D. J. 2009, *ApJ*, **707**, 916
 Fixsen, D. J., Cheng, E. S., Gales, J. M., et al. 1996, *ApJ*, **473**, 576
 Follin, B., & Knox, L. 2017, arXiv:1707.01175
 Font-Ribera, A., Kirkby, D., Busca, N., et al. 2014, *JCAP*, **5**, 027
 Freedman, W. L., Madore, B. F., Scowcroft, V., et al. 2012, *ApJ*, **758**, 24
 Gelman, A., & Rubin, D. B. 1992, *StaSc*, **7**, 457
 Heavens, A., Fantaye, Y., Sellentin, E., et al. 2017, *PhRvL*, **119**, 101301
 Hildebrandt, H., Viola, M., Heymans, C., et al. 2017, *MNRAS*, **465**, 1454
 Hinshaw, G., Larson, D., Komatsu, E., et al. 2013, *ApJS*, **208**, 19
 Hong, T., Han, J. L., & Wen, Z. L. 2016, *ApJ*, **826**, 154
 Hou, Z., Reichardt, C. L., Story, K. T., et al. 2014, *ApJ*, **782**, 74
 Izotov, Y. I., Thuan, T. X., & Guseva, N. G. 2014, *MNRAS*, **445**, 778
 Joudaki, S., Blake, C., Heymans, C., et al. 2017, *MNRAS*, **465**, 2033
 Kazin, E. A., Koda, J., Blake, C., et al. 2014, *MNRAS*, **441**, 3524
 Köhlinger, F., Viola, M., Joachimi, B., et al. 2017, *MNRAS*, **471**, 4412
 Lewis, A., & Bridle, S. 2002, *PhRvD*, **66**, 103511
 Louis, T., Grace, E., Hasselfield, M., et al. 2017, *JCAP*, **6**, 031
 Maruccci, L. E., Mangano, G., Kievsky, A., & Viviani, M. 2016, *PhRvL*, **116**, 102501
 Peimbert, A., Peimbert, M., & Luridiana, V. 2016, *RMxAA*, **52**, 419
 Percival, W. J., Ross, A. J., Sánchez, A. G., et al. 2014, *MNRAS*, **439**, 2531
 Pettini, M., & Cooke, R. 2012, *MNRAS*, **425**, 2477
 Planck Collaboration, Ade, P. A. R., Aghanim, N., et al. 2016a, *A&A*, **594**, A13
 Planck Collaboration, Aghanim, N., Akrama, Y., et al. 2017, *A&A*, **607**, A95
 Planck Collaboration, Aghanim, N., Arnoud, M., et al. 2016c, *A&A*, **594**, A11
 Planck Collaboration, Aghanim, N., Ashdown, M., et al. 2016b, *A&A*, **596**, A107
 Reid, B., Ho, S., Padmanabhan, N., et al. 2016, *MNRAS*, **455**, 1553
 Riemer-Sørensen, S., Kotuš, S., Webb, J. K., et al. 2017, *MNRAS*, **468**, 3239
 Riemer-Sørensen, S., & Sem Jensen, E. 2017, arXiv:1705.03653
 Riess, A. G., Macri, L., Casertano, S., et al. 2009, *ApJ*, **699**, 539
 Riess, A. G., Macri, L., Casertano, S., et al. 2011, *ApJ*, **730**, 119
 Riess, A. G., Macri, L. M., Hoffmann, S. L., et al. 2016, *ApJ*, **826**, 56
 Ross, A. J., Samushia, L., Howlett, C., et al. 2015, *MNRAS*, **449**, 835
 Sherwin, B. D., van Engelen, A., Sehgal, N., et al. 2017, *PhRvD*, **95**, 123529
 Sievers, J. L., Hlozek, R. A., Nolte, M. R., et al. 2013, *JCAP*, **10**, 60
 Slosar, A., Iršič, V., Kirkby, D., et al. 2013, *JCAP*, **4**, 026
 Story, K. T., Reichardt, C. L., Hou, Z., et al. 2013, *ApJ*, **779**, 86
 Thornton, R. J., Ade, P. A. R., Aiola, S., et al. 2016, *ApJS*, **227**, 21
 van Engelen, A., Keisler, R., Zahn, O., et al. 2012, *ApJ*, **756**, 142
 Veropalumbo, A., Marulli, F., Moscardini, L., Moresco, M., & Cimatti, A. 2016, *MNRAS*, **458**, 1909
 Wang, Y., Xu, L., & Zhao, G.-B. 2017, *ApJ*, **849**, 84
 Weinberg, D. H., Mortonson, M. J., Eisenstein, D. J., et al. 2013, *PhR*, **530**, 87
 Zhang, B. R., Childress, M. J., Davis, T. M., et al. 2017, *MNRAS*, **471**, 2254